

ARTICLE



An adaptive least-squares finite element method for Giesekus viscoelastic flow problems

Hsueh-Chen Lee^a and Hyesuk Lee^b

^aGeneral Education Center, Wenzao Ursuline University of Languages, Kaohsiung, Taiwan; ^bSchool of Mathematical and Statistical Sciences, Clemson University, Clemson, SC, USA

ABSTRACT

In this study, a least-squares (LS) finite element method with an adaptive mesh approach is investigated for Giesekus viscoelastic flow problems. We consider the weighted LS method on uniform and adaptive meshes for the Newton linearized viscoelastic problem, where adaptive grids are automatically generated by the least-squares solutions. We use a residual-type a-posteriori error estimator to adjust weights in the LS functional and compare the convergence behaviour of adaptive meshes generated using different grading functions. Numerical results demonstrate that the adaptive LS method shows at least the first-order convergence rate when equal-order linear interpolation functions are used for all variables, which agrees with the theoretical estimate. In addition, adaptive grids generated using the velocity outperform those based on the a-posteriori error estimator, yielding better numerical results.

ARTICLE HISTORY

Received 19 July 2020 Revised 16 October 2020 Accepted 3 December 2020

KEYWORDS

Least-squares; adaptive mesh; a-posteriori error; viscoelastic fluid; 4-to-1 planar contraction

2010 MATHEMATICS SUBJECT CLASSIFICATIONS 65N50; 76M10; 65N30

1. Introduction

The objective of this study is to develop an adaptive least-squares (LS) finite element method for Giesekus viscoelastic flow problems. The Giesekus model gained prominence because the model reproduces numerous rheology characteristics of polymer solutions and other liquids [16]. There have been many numerical algorithms proposed to simulate viscoelastic flow problems [1,3–5,9,10,18]. However, the numerical approximation of viscoelastic flows is still limited and known to be challenging with many issues such as improper boundary conditions, hyperbolic nature of the equations, loss of convergence for high values of the Weissenberg number [5,8] and so on. The 4-to-1 contraction flow problem is a well-known benchmark problem for the study of viscoelastic flow behaviour, where the flow path suddenly changes its geometry, especially in two-dimensional systems [17]. Additional difficulties arise in solving such flow problems; for example, geometric discontinuities cause corner singularities, therefore, a refined mesh should be used near the reentrance corner.

To resolve these problems, LS methods with adaptive meshes have been extensively used as powerful tools for more efficient and accurate results [3,11-13]. For the formulation of weighted LS methods, the extra-stress tensor for viscoelastic fluid is split into its elastic and viscous components and the L^2 -norm of the residual of the continuity equation is multiplied by an appropriately adjusted weight [5,9,10]. In our previous research [5,9], LS methods with nonlinear weights (NWLS) are used for viscoelastic fluid flows at low Weissenberg number past a 4-to-1 contraction, and in [10,15] adaptive weights for mass conservation are considered based on an LS functional. In [6], an a-posteriori

error estimate is provided by a weighted LS functional and used to guide adaptive refinements. In [11], an a-posteriori error estimator is presented for a linear problem in the general setting and used for adaptive mesh refinements in numerical tests. Cai and Westphal present an adaptive mixed LS finite element method in [3] to analyse steady Oldroyd-type viscoelastic fluids, where a nonlinear LS functional is used for adaptive mesh refinement. Their algorithms select elements to be refined for optimal computational efficiency, considering both error reduction and computational cost. The adaptive LS approach in [12] uses a grading function of velocity magnitude to refine the mesh adaptively for Carreau generalized Newtonian fluid flows. In [13], adaptive LS approaches generate optimally graded grids to redistribute the mesh adaptively for the Stokes equation based on the stress and vorticity formulation. The results indicate, using the hybrid adaptive mesh that combines graded and regular grids, optimal convergence rate in all variables is obtained and the grids effects can be reduced [13]. In [10], the LS method with two stabilized weights is applied to a flow through the slot channel. The a-posteriori error estimator serves as an indicator to adjust the weight for the continuity equation in the LS functional. This approach improves mass conservation and yields convergence at

On the basis of the aforementioned studies, in this study, we develop an adaptive LS (ALS) method for viscoelastic fluid flows governed by the Giesekus model. The LS approach in [10] is considered here instead of the NWLS method [5,9] due to its relative simplicity, with optimally chosen weights by numerical tests. We consider the coercivity and continuity properties for the LS functional, from which an error estimate for the Newton linearized problem follows by the similar argument in [3,10]. The error estimate is verified through convergence tests for a non-physical problem with a known solution, using properly adjusted weights for the LS functional and grading functions for mesh refinement. The proposed method is also applied to simulate the 4-to-1 contraction problem and to investigate the physical parameter effects. Low order basis functions and adaptive grids in high gradient regions are considered to improve solution accuracy and reduce the size of the linearized system of equations. We employ the adaptive mesh algorithm in [12] using grading functions generated by the velocity and an a-posteriori error estimator, respectively, to capture high gradient regions in the flow domain and compare numerical results by two different grading functions.

high Weissenberg numbers when low order basis functions are used.

The organization of this paper is as follows. Section 2 introduces notation and the model equations. Section 3 presents the coercivity and continuity estimates of the LS functional. Section 4 provides the error estimate of the LS approximations, and describes the adaptive mesh approach and numerical implementation. Section 5 provides numerical results for numerical examples and finally conclusions follow in Section 6.

2. Notation and model equations

The governing equations are solved on a square test domain and a 4-to-1 contraction domain, with boundaries labelled as shown in Figure 1. Let Ω be a bounded and connected domain in \mathbb{R}^d with d=2 and Lipschitz boundary Γ , where $\Gamma=\Gamma_{\text{in}}\cup\Gamma_{\text{wall}}\cup\Gamma_{\text{out}}\cup\Gamma_{\text{sym}}$. The $\Gamma_{\text{in}},\Gamma_{\text{wall}},\Gamma_{\text{out}}$ and Γ_{sym} are the inlet, wall, outlet and symmetric boundaries, respectively. Consider the steady-state, incompressible flow governed by

$$\rho(\mathbf{u} \cdot \nabla \mathbf{u}) - \nabla \cdot \boldsymbol{\tau} + \nabla p = \mathbf{f} \quad \text{in } \Omega, \tag{1}$$

$$\nabla \cdot \mathbf{u} = 0 \quad \text{in } \Omega, \tag{2}$$

where ρ is the density, **f** is the body force vector, the unknowns **u** and τ are the velocity and the extrastress tensor, respectively, and p is the scalar pressure. We assume that the pressure p is fixed to p_0 at the point \mathbf{x}_0 on Γ , i.e. $p(\mathbf{x}_0) = p_0$, in order to ensure the uniqueness of pressure. The extra-stress is written as a superposition of the polymeric and viscous stresses [5], i.e.

$$\tau = \tau_p + \tau_s$$

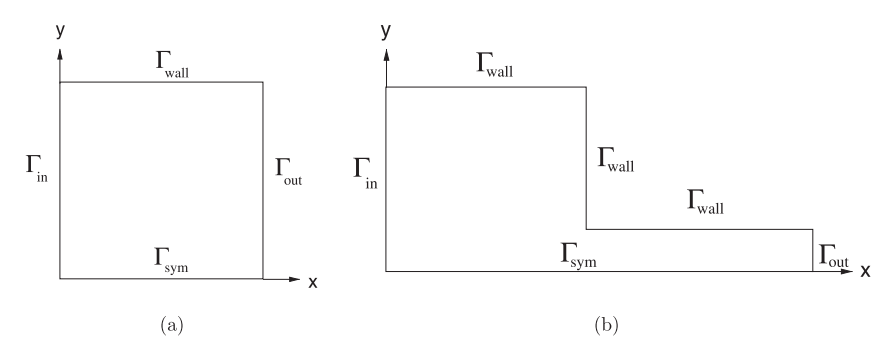


Figure 1. Computational domains: (a) square test domain, (b) 4-to-1 contraction domain.

The viscous stress is Newtonian, i.e.

$$\tau_{s} = 2\eta_{s} \mathbf{D}(\mathbf{u}),\tag{3}$$

where η_s is a constant viscosity and $\mathbf{D}(\mathbf{u}) = 0.5(\nabla \mathbf{u} + \nabla \mathbf{u}^T)$ is the standard strain rate tensor. For viscoelastic flows represented by the Giesekus model, the polymer contribution to the stress obeys the following constitutive equation [5]:

$$\boldsymbol{\tau}_p + \frac{\alpha \lambda}{\eta_p} (\boldsymbol{\tau}_p \cdot \boldsymbol{\tau}_p) + \lambda (\mathbf{u} \cdot \nabla \boldsymbol{\tau}_p - A(\nabla \mathbf{u}, \boldsymbol{\tau}_p)) = 2\eta_p \mathbf{D}(\mathbf{u}), \tag{4}$$

where

$$A(\nabla \mathbf{u}, \boldsymbol{\tau}_p) := (\nabla \mathbf{u})^T \boldsymbol{\tau}_p + \boldsymbol{\tau}_p \nabla \mathbf{u}.$$

In (4), λ is a relaxation time which is a measure of the time taken for the stress to relax. η_p is the polymeric contribution to the viscosity, and α is called the mobility factor. The Giesekus model with $\alpha > 0$ predicts a shear-thinning viscosity and non-vanishing first and second normal stress differences in viscometric flows, a finite extensional viscosity for all values of the extensional rate, and stress-overshoot in start-up flows in [7]. With $\alpha > 0$, shear-thinning is always observed. The $\alpha \in [0,1]$ factor is required as discussed in [7] and setting $\alpha = 0$ reduces the model to the Oldroyd-B model.

Collecting (1)-(4) and nondimensionalizing the equations, we have the Giesekus flow model written as

$$Re(\mathbf{u} \cdot \nabla \mathbf{u}) - \nabla \cdot \boldsymbol{\tau}_{p} - \nabla \cdot \boldsymbol{\tau}_{s} + \nabla p = \mathbf{f} \quad \text{in } \Omega,$$
 (5)

$$\nabla \cdot \mathbf{u} = 0 \quad \text{in } \Omega, \tag{6}$$

$$\boldsymbol{\tau}_{s} - 2\beta \mathbf{D}(\mathbf{u}) = \mathbf{0} \quad \text{in } \Omega, \tag{7}$$

$$\boldsymbol{\tau}_{p} + We(\mathbf{u} \cdot \nabla \boldsymbol{\tau}_{p} - A(\nabla \mathbf{u}, \boldsymbol{\tau}_{p})) + \frac{\alpha We}{(1 - \beta)} (\boldsymbol{\tau}_{p} \cdot \boldsymbol{\tau}_{p})$$
$$-2(1 - \beta)\mathbf{D}(\mathbf{u}) = \mathbf{0} \quad \text{in } \Omega, \tag{8}$$

where Re is the Reynolds number, $Re \equiv LU\rho/\eta_0$, in which $\eta_0 = \eta_s + \eta_p$ is the zero-shear-rate viscosity, L and U are the characteristic length and velocity, respectively. $\beta = \eta_s/\eta_0 \in [0,1]$ is the ratio of solvent viscosity to the total zero-shear-rate viscosity. β is set to 1/9 in the present work as typically used in the literature. The Weissenberg number We > 0 is the concepts of elasticity, $We \equiv \lambda U/L$, and in the case of We = 0, the model reduces to the Newtonian model, the Navier–Stokes equations.

To simplify the formulation of LS method and its presentation, a homogeneous boundary condition is assumed for \mathbf{u} , $\mathbf{u} = \mathbf{0}$ on $\Gamma \setminus \Gamma_{\text{sym}}$. On the axis of symmetry Γ_{sym} , we assume the standard symmetric boundary conditions: $\mathbf{u} \cdot \mathbf{n} = 0$ and $\pi : \mathbf{n} \otimes \mathbf{t} = \mathbf{0}$, where \mathbf{n} , \mathbf{t} are outward unit normal and tangential vectors, respectively, and $\pi = \tau - p\mathbf{I}$ is the Cauchy stress tensor, where \mathbf{I} is the identity matrix. Problems with nonhomogeneous boundary conditions on Γ_{in} and Γ_{out} will be considered for numerical tests of 4-to-1 contraction flows, which can be formulated in an analogous manner.

3. Least squares functional

Let $H^s(\Omega)$, $s \ge 0$, be the Sobolev spaces with the standard associated inner products $(\cdot, \cdot)_s$ and their respective norms $\|\cdot\|_s$. For s = 0, $H^s(\Omega)$ coincides with $L^2(\Omega)$. The function spaces used in our formulations are defined as

$$\mathbf{V} := \{ \mathbf{v} \mid \mathbf{v} \in (H^1(\Omega))^2, \mathbf{v} = \mathbf{0} \text{ on } \Gamma \setminus \Gamma_{\text{sym}}, \mathbf{v} \cdot \mathbf{n} = 0 \text{ on } \Gamma_{\text{sym}} \},$$

$$Q := H^1(\Omega),$$

$$\Sigma_s := \{ \boldsymbol{\sigma} \mid \boldsymbol{\sigma} \in (H^1(\Omega))^{2 \times 2}, \, \boldsymbol{\sigma}^T = \boldsymbol{\sigma} \}, \, \Sigma_p := \Sigma_s,$$

and let the product space $\Phi := \mathbf{V} \times Q \times \Sigma_s \times \Sigma_p$.

To define the least squares functional, we first consider Newton linearization of the nonlinear flow equations (5)–(8) about known approximations \mathbf{u}_{ℓ} , $\boldsymbol{\tau}_{p_{\ell}}$ of the velocity and the polymeric stress tensor, respectively. Using the following notation:

$$\mathbf{f_1} := Re(\mathbf{u}_{\ell} \cdot \nabla \mathbf{u}_{\ell}) + \mathbf{f}, \tag{9}$$

$$B(\mathbf{u}, \tau_p) := We\left(\mathbf{u} \cdot \nabla \tau_{p_{\ell}} - A(\nabla \mathbf{u}_{\ell}, \tau_p) - A(\nabla \mathbf{u}, \tau_{p_{\ell}})\right), \tag{10}$$

$$G(\tau_{p}) := (\alpha We/(1-\beta)) \left(\tau_{p_{\ell}} \cdot \tau_{p} + \tau_{p} \cdot \tau_{p_{\ell}} \right), \tag{11}$$

$$\mathbf{f}_2 := We \left(\mathbf{u}_{\ell} \cdot \nabla \boldsymbol{\tau}_{p_{\ell}} - A(\nabla \mathbf{u}_{\ell}, \boldsymbol{\tau}_{p_{\ell}}) \right) + (\alpha We/(1 - \beta))(\boldsymbol{\tau}_{p_{\ell}} \cdot \boldsymbol{\tau}_{p_{\ell}}), \tag{12}$$

the linearized system can be written as

$$Re(\mathbf{u}_{\ell} \cdot \nabla \mathbf{u} + \mathbf{u} \cdot \nabla \mathbf{u}_{\ell}) - \nabla \cdot \boldsymbol{\tau}_{p} - \nabla \cdot \boldsymbol{\tau}_{s} + \nabla p = \mathbf{f}_{1} \text{ in } \Omega,$$
 (13)

$$\nabla \cdot \mathbf{u} = 0 \text{ in } \Omega, \tag{14}$$

$$\tau_s - 2\beta \mathbf{D}(\mathbf{u}) = \mathbf{0} \text{ in } \Omega, \tag{15}$$

$$\boldsymbol{\tau}_{p} + We\left(\mathbf{u}_{\ell} \cdot \nabla \boldsymbol{\tau}_{p}\right) + B(\mathbf{u}, \boldsymbol{\tau}_{p}) + G(\boldsymbol{\tau}_{p}) - 2(1 - \beta)\mathbf{D}(\mathbf{u}) = \mathbf{f}_{2} \text{ in } \Omega.$$
 (16)

We now define the least-squares (LS) functional for (13)–(16) by

$$J(\mathbf{U}; \mathbf{F}) = \|Re(\mathbf{u}_{\ell} \cdot \nabla \mathbf{u} + \mathbf{u} \cdot \nabla \mathbf{u}_{\ell}) - \nabla \cdot \boldsymbol{\tau}_{s} - \nabla \cdot \boldsymbol{\tau}_{p} + \nabla p - \mathbf{f}_{1}\|_{0}^{2}$$

$$+ K \|\nabla \cdot \mathbf{u}\|_{0}^{2} + \|\boldsymbol{\tau}_{s} - 2\beta \mathbf{D}(\mathbf{u})\|_{0}^{2}$$

$$+ W \|\boldsymbol{\tau}_{p} + We(\mathbf{u}_{\ell} \cdot \nabla \boldsymbol{\tau}_{p}) + B(\mathbf{u}, \boldsymbol{\tau}_{p}) + G(\boldsymbol{\tau}_{p}) - 2(1 - \beta)\mathbf{D}(\mathbf{u}) - \mathbf{f}_{2}\|_{0}^{2}$$

$$(17)$$

 $\forall \mathbf{U}=(\mathbf{u},p,\pmb{\tau}_s,\pmb{\tau}_p)\in\Phi,$ and the LS minimization problem for the solution of system is given by: $\mathbf{U}\in\Phi$ such that

$$J(\mathbf{U}; \mathbf{F}) = \inf_{\mathbf{V} \in \Phi} J(\mathbf{V}; \mathbf{F}). \tag{18}$$

The weight W > 0 is introduced to stabilize the LS functional at a high We and α in the constitutive equation. We consider the weight given by

$$W = (1 + We + s\alpha)^2, \tag{19}$$

where $-1 \le s \le 1$ for We > 0 and $0 \le \alpha \le 1$ in the Giesekus model. In [4,5,9], appropriately designed weights involving We are employed for the NWLS and Galerkin least squares methods to solve

Oldroyd-B and Giesekus models at high We. The weight W in (19), which is in a simpler form than the nonlinear weight of the NWLS method [5], will be considered in the current study. The Giesekus model with $0 \le \alpha \le 1$ is considered here because $\alpha > 0$ always leads to shear-thinning. The α factor predicts a shear-thinning viscosity, which decreases with increasing shear rate. To appropriately adjust constants s in the weight value W for reflecting α , we consider testing with various s = -1, 0,and 1. In this work, we use convergence rates of the a-posteriori error estimate for the LS solutions as an indicator to adjust the constant s. Several different parameter values for We and α in the Giesekus model will be also considered for numerical tests in Section 5.

The positive constant $K = 10^m$, where m ranges from 0 to 10, is chosen for the continuity equations based on [9,12], where LS solutions are improved by the sufficiently weighted mass conservation term. In this work, we consider an a-posteriori error estimate for the first-order system as an indicator to adjust the weight K, as in [12,15].

Denote two norms on Φ as

$$\||\mathbf{U}|\| = \left(\|\mathbf{u}\|_{1}^{2} + \|p\|_{0}^{2} + \|\tau_{s}\|_{0}^{2} + \|\tau_{p}\|_{0}^{2}\right)^{1/2}$$
(20)

and

$$\||\mathbf{U}|\|_{1} = \left(Re^{2} \|\mathbf{u}\|_{1}^{2} + \|p\|_{1}^{2} + \|\boldsymbol{\tau}_{s}\|_{1}^{2} + \|\boldsymbol{\tau}_{p}\|_{1}^{2}\right)^{1/2}$$
(21)

 $\forall \mathbf{U} = (\mathbf{u}, p, \boldsymbol{\tau}_s, \boldsymbol{\tau}_p) \in \Phi.$

We derived coercivity and continuity estimates for a homogeneous functional designed for the linear Phan-Thien-Tanner (PTT) viscoelastic fluid model in [10]. Replacing the second term of (4) by $\frac{\alpha \lambda}{\eta_p} tr(\tau_p) \tau_p$ is the linear PTT model. Coercivity and continuity of (17) can be shown by a similar approach, therefore, we present the next theorem without proof. See [10] for details.

Theorem 3.1: Suppose the known approximations \mathbf{u}_{ℓ} , $\boldsymbol{\tau}_{p_{\ell}}$ are uniformly bounded satisfying $\nabla \cdot \mathbf{u}_{\ell} =$ 0 and

$$M := \max\{\|\mathbf{u}_{\ell}\|_{\infty}, \|\nabla \mathbf{u}_{\ell}\|_{\infty}, \|\boldsymbol{\tau}_{p_{\ell}}\|_{\infty}, \|\nabla \boldsymbol{\tau}_{p_{\ell}}\|_{\infty}\} < \infty.$$
 (22)

Then, for any $\mathbf{U} = (\mathbf{u}, p, \tau_s, \tau_p) \in \Phi$, there are positive constants, c_0 and c_1 , which depend on Ω , β , We, α , and M, such that

$$c_0 \| \|\mathbf{U}\|^2 < J(\mathbf{U}; \mathbf{0}) < c_1 \| \|\mathbf{U}\|_1^2,$$
 (23)

if M is sufficiently small.

4. Adaptive finite element approximation

For the finite element approximation, we assume that the domain Ω is a polygon and that \mathcal{T}_h is a collection of finite elements such that $\Omega = \bigcup_{T \in \mathcal{T}_h} T$ with $h = \max\{\text{diam}(T) : T \in \mathcal{T}_h\}$. Assume that the triangulation \mathcal{T}_h is shape-regular and satisfies the assumption for inverse estimates [9]. The grid size is defined as $h = 2\sqrt{A}/\sqrt{N}$, where A is the area of the domain and N is the number of elements in \mathcal{T}_h . Let $P_r(T)$ denote the space of polynomials of degree less than or equal to r on element T. Define finite element spaces for the approximate of $(\mathbf{u}, p, \tau_s, \tau_p)$ by

$$\mathbf{V}^{h} = \{\mathbf{v}^{h} \mid \mathbf{v}^{h} \in \mathbf{V} \cap (C^{0}(\Omega))^{2}, \ \mathbf{v}^{h} \mid_{T} \in P_{r+1}(T)^{2} \ \forall T \in \mathcal{T}_{h}\},$$

$$Q^{h} = \{q^{h} \mid q^{h} \in Q \cap C^{0}(\Omega), \ q^{h} \mid_{T} \in P_{r+1}(T) \ \forall T \in \mathcal{T}_{h}\},$$

$$\Sigma^{h}_{s} = \{\boldsymbol{\sigma}^{h} \mid \boldsymbol{\sigma}^{h} \in \Sigma_{s} \cap (C^{0}(\Omega))^{2 \times 2}, \ \boldsymbol{\sigma}^{h} \mid_{T} \in P_{r+1}(T)^{2 \times 2} \ \forall T \in \mathcal{T}_{h}\},$$

$$\Sigma^{h}_{p} = \{\boldsymbol{\sigma}^{h} \mid \boldsymbol{\sigma}^{h} \in \Sigma_{p} \cap (C^{0}(\Omega))^{2 \times 2}, \ \boldsymbol{\sigma}^{h} \mid_{T} \in P_{r+1}(T)^{2 \times 2} \ \forall T \in \mathcal{T}_{h}\}.$$

Let $\Phi^h := \mathbf{V}^h \times Q^h \times \Sigma^h_s \times \Sigma^h_p$ be finite element subspaces of Φ with the following approximation properties. Let $S^h = \{u \in C^0(\Omega) : u|_T \in P_{r+1}(T) \ \forall T \in T_h\}$ admit the property

$$\inf_{u^h \in \mathbb{S}^h} \left\| u - u^h \right\|_{l} \le Ch^m \left\| u \right\|_{m+l} \forall u \in H^{m+l} \left(\Omega \right), \tag{24}$$

for m < r + 1 and l = 0, 1.

Then, the discrete least squares problem for the linearized Giesekus viscoelastic fluid is to choose $\mathbf{U}^h \in \Phi^h$ such that

$$J(\mathbf{U}^h; \mathbf{F}) = \inf_{\mathbf{V}^h \in \Phi^h} J(\mathbf{V}^h; \mathbf{F}), \tag{25}$$

where $\mathbf{U}^h = (\mathbf{u}^h, p^h, \boldsymbol{\tau}_s^h, \boldsymbol{\tau}_p^h)$ and $\mathbf{V}^h = (\mathbf{v}^h, q^h, \boldsymbol{\sigma}_s^h, \boldsymbol{\sigma}_p^h)$. Derivation of the following a-priori error estimate for the solution of (25) is standard and straightforward using Theorem 3.1 and the approximation property (24).

Theorem 4.1: Consider approximating the solution to (13)–(16) through the discrete minimization problem (25) under the assumptions in (22). Assume that $\mathbf{U} \in \Phi \cap (H^{m+1}(\Omega))^2 \times H^{m+1}(\Omega) \times H^{m+1}(\Omega)$ $(H^{m+1}(\Omega))^{2\times 2}\times (H^{m+1}(\Omega))^{2\times 2}$ is the solution to (18) and M is small, then the solution $\mathbf{U}^h\in\Phi^h$ to (25) satisfies

$$\| |\mathbf{U} - \mathbf{U}^h| \| \le Ch^m (\|\mathbf{\tau}_s\|_{m+1} + \|\mathbf{\tau}_p\|_{m+1} + \|p\|_{m+1} + Re \|\mathbf{u}\|_{m+1}),$$
 (26)

for $m \leq r + 1$.

Proof: The coercivity and continuity properties of (17) in Theorem 3.1 yield

$$\left\| \left| \mathbf{U}^h - \mathbf{U} \right| \right\| \leq \inf_{\mathbf{V}^h \in \mathbf{\Phi}^h} \frac{c_1}{c_0} \left\| \left| \mathbf{V}^h - \mathbf{U} \right| \right\|_1,$$

which implies the error estimate (26) using (24).

Note that the use of continuous piecewise linear polynomials for all unknowns yields the error estimates

$$\| |\mathbf{U} - \mathbf{U}^h| \| \le Ch (\|\mathbf{\tau}_s\|_2 + \|\mathbf{\tau}_p\|_2 + \|p\|_2 + Re \|\mathbf{u}\|_2).$$
 (27)

The theoretical a-priori error bound is only O(h) in the linearized functional norm $J^{1/2}$ in (17), O(h)in the L^2 -norm for τ_s , τ_p , and p, and O(h) in the H^1 -norm for \mathbf{u} .

The solution of the nonlinear systems in (5)-(8) is approximated by a sequence of the linearized system (13)-(16). The LS approach to the linearized system (13)-(16) provides an iterative procedure as follows: for a chosen initial approximation \mathbf{U}_0^h seek approximations $\mathbf{U}_{\ell+1}^h \in \Phi^h$ for $\ell = 0, 1, 2, 3, \dots$ satisfying

$$J_{\ell}(\mathbf{U}_{\ell}^{h};\mathbf{F}) = \inf_{\mathbf{V}^{h} \in \Phi^{h}} J_{\ell}(\mathbf{V}^{h};\mathbf{F}), \tag{28}$$

where the LS functional $I_{\ell}(\mathbf{U}; \mathbf{F})$ is defined as

$$J_{\ell}(\mathbf{U}; \mathbf{F}) = \|Re(\mathbf{u}_{\ell} \cdot \nabla \mathbf{u} + \mathbf{u} \cdot \nabla \mathbf{u}_{\ell}) - \nabla \cdot \boldsymbol{\tau}_{s} - \nabla \cdot \boldsymbol{\tau}_{p} + \nabla p - \mathbf{f}_{1}\|_{0}^{2}$$

$$+ K \|\nabla \cdot \mathbf{u}\|_{0}^{2} + \|\boldsymbol{\tau}_{s} - 2\beta \mathbf{D}(\mathbf{u})\|_{0}^{2}$$

$$+ W \|\boldsymbol{\tau}_{p} + We(\mathbf{u}_{\ell} \cdot \nabla \boldsymbol{\tau}_{p}) + B(\mathbf{u}, \boldsymbol{\tau}_{p}) + G(\boldsymbol{\tau}_{p}) - 2(1 - \beta)\mathbf{D}(\mathbf{u}) - \mathbf{f}_{2}\|_{0}^{2},$$

$$(29)$$

and $\mathbf{f_1}$, $B(\mathbf{u}, \tau_p)$, $G(\tau_p)$, and $\mathbf{f_2}$ are given as (9)–(12).

We now consider the following nonlinear LS functional of the residual of the system (5)–(8):

$$g(\mathbf{U}^{h}) = \|Re(\mathbf{u}^{h} \cdot \nabla \mathbf{u}^{h}) - \nabla \cdot \boldsymbol{\tau}_{p}^{h} - \nabla \cdot \boldsymbol{\tau}_{s}^{h} + \nabla p^{h} - \mathbf{f}\|_{0}^{2}$$

$$+ \|\nabla \cdot \mathbf{u}^{h}\|_{0}^{2} + \|\boldsymbol{\tau}_{s}^{h} - 2\beta \mathbf{D}(\mathbf{u}^{h})\|_{0}^{2}$$

$$+ \|\boldsymbol{\tau}_{p}^{h} + We(\mathbf{u}^{h} \cdot \nabla \boldsymbol{\tau}_{p}^{h} - A(\nabla \mathbf{u}^{h}, \boldsymbol{\tau}_{p}^{h})) + \frac{\alpha We}{(1-\beta)} (\boldsymbol{\tau}_{p}^{h} \cdot \boldsymbol{\tau}_{p}^{h}) - 2(1-\beta)\mathbf{D}(\mathbf{u}^{h})\|_{0}^{2}. \tag{30}$$

The nonlinear LS functional norm $g^{1/2}$ is an a-posteriori error for the system of governing equations, which will be used as an indicator to adjust the weight K in numerical tests. When the lower basis functions are considered to approximate all unknowns, we expect that the error $g^{1/2}$ is in the order of O(h) if the stopping tolerance for the above iterative process is small enough, and this will be verified by numerical tests in Section 5. Also the a-posteriori error will be used in a refinement process to illustrate the convergence of the adaptive method.

Next we consider an adaptive mesh approach for viscoelastic flow problems. In [12], we developed an adaptively refined algorithm for the generalized Newtonian fluid flows, which adds new grids in the high gradient region, maintaining the solution accuracy in the low gradient region. This approach uses a grading function of velocity magnitude to refine the mesh adaptively. The results in [12] indicate that adaptive meshes generated by the grading function automatically refine local grids for the generalized Newtonian fluid flows, and the refinement results for various parameter values are satisfactory. However, in [13], the grid effects are observed in convergence of the LS solutions; the convergence behaviour is mesh dependent. Multiple triangular grids are used in the LS method to reduce the grid effects for planar contraction flows [9,13]. The results indicate that, when recirculating flows exist in the flow field, directional Delaunay triangular grids are unsuitable for the LS method. By contrast, for planar flow problems, the longest edges of these triangular grids along the same direction are more suitable for the LS method, as demonstrated in [13]. Therefore, to capture the flow region of the Giesekus model in our study, we develop a multi-grid approach based on the LS method. The mesh is initialized using the adaptive mesh algorithm in [12], by using the grading function ϕ_T on elements T of a mesh T given by $\phi_T = |\nabla q|_T$, where the scalar function q is calculated based in the LS solutions. The magnitudes of velocity $|\mathbf{u}| = \sqrt{u_1^2 + u_2^2}$ and a nonlinear LS functional norm $g^{1/2}$ in (30) are considered as the function q ($q = |\mathbf{u}|$ and $q = g^{1/2}$) for the mesh redistribution function $f(\phi_T)$ in [12], defined by

$$f(\phi_T) = |T|_{\text{max}} - \left(\phi_T - \phi_{T_{\text{min}}}\right) \frac{\Delta |T|}{\Delta \phi_T},$$

where $|T|_{\max} = \max\{|T| : \forall T \in \mathcal{T}\}, \ \Delta|T| = |T|_{\max} - |T|_{\min} \text{ and } \Delta\phi_T = \phi_{T_{\max}} - \phi_{T_{\min}}.$ If $T \in \mathcal{T}$ satisfies $f(\phi_T) \leq |T|$, then T is subdivided.

Then, we modify triangular mesh of the downstream region by aligning the longest edges of these triangular grids in the same direction downstream. In numerical experiments discussed in the next section, multiple triangular grids are applied to Giesekus viscoelastic planar contraction flows by using the LS method.

5. Numerical results

We consider two numerical examples. The first problem is chosen for convergence tests with the known exact solution in the unit square domain, and the second is a 4-to-1 contraction flow problem. Due to the symmetry along y = 0, two computation domains are reduced to half. All variables are approximated by P_1 polynomials, and the initial \mathbf{u}_ℓ and $\boldsymbol{\tau}_{p\ell}$ for Newton linearization are set to zero in all computations.

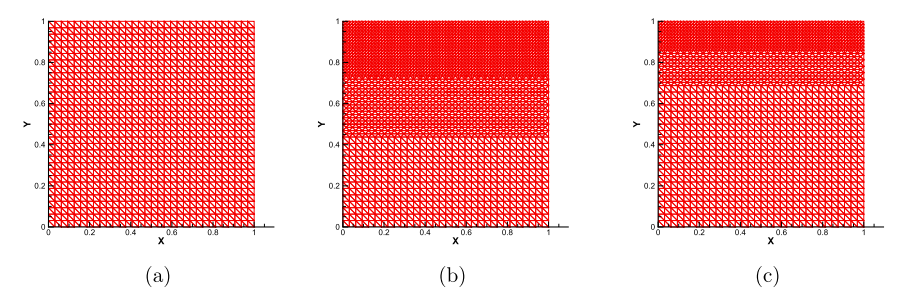


Figure 2. (a) Initial Mesh D with 32 partitions per unit length. (b) Mesh A after two refinement steps from Mesh D using $|\mathbf{u}|$. (c) Mesh B after two refinement steps from Mesh D using $q^{1/2}$.

5.1. Problem 1

Consider the flow in a planar channel on the domain $[0,1] \times [0,1]$ with the line of symmetry along y = 0. Let $\mathbf{u} = (u_1, u_2)$ be specified along the boundary except on the axis of symmetry, and τ_p be specified on the inflow boundary where $\mathbf{u} \cdot \mathbf{n} < 0$. The pressure p = -1 is set at the point (1, 0), and u_2 and $\tau_{p_{XY}}$ vanish on the axis of symmetry. The exact solution is chosen as

$$\mathbf{u} = \begin{bmatrix} 1 - y^4 \\ 0 \end{bmatrix}, \quad p = -x^2, \quad \boldsymbol{\tau}_p = \begin{bmatrix} 2 \operatorname{We}(1 - \beta) \left(\frac{\partial u_1}{\partial y} \right)^2 & (1 - \beta) \frac{\partial u_1}{\partial y} \\ (1 - \beta) \frac{\partial u_1}{\partial y} & 0 \end{bmatrix},$$

where τ_p represents the analytical solution for the Oldroyd-B model in steady-state shear flow [2]. The source terms in (5) and (8) are chosen appropriately for the exact solution, as shown in [5]. The modelling parameters are selected as (Re, We, α , β) = (1, 0.2, 0.2, 1/9) and the weight parameter s = -1 is used for the W in (19).

The meshes considered are illustrated in Figure 2. The uniform triangular Mesh D in Figure 2(a) is the mesh generated using Delaunay triangular grids with 32 partitions per unit length. The adaptive Meshes A and B in Figures 2(b) and 2(c) are generated using the magnitude of velocity, $|\mathbf{u}|$, and the nonlinear LS functional norm $g^{1/2}$, respectively. The stopping criterion for mesh convergence is given by $\|g_{j+1}^{1/2} - g_j^{1/2}\|/\|N_{j+1} - N_j\| < 10^{-6}$, where N_j is the number of elements at the jth refinement step. First, in order to appropriately adjust the weight $K=10^m$ in (17), Mesh D is initially used. We iterate m, where m ranges from 1 to 10, to investigate convergence of the functional $g^{1/2}$ in (30), as shown in [10]. The convergence of the iteration scheme with $K=10^m$ is declared when the relative norm of residual in the nonlinear functional between two consecutive iterations, $\delta g_m^{1/2} := \|g_{m+1}^{1/2} - g_m^{1/2}\|/\|g_{m+1}^{1/2}\|$, is less than 10^{-4} . We observe that convergence is achieved at m=6, therefore, the mass conservation weight $K=10^6$ is used in the LS formulation for all computations in the first example.

To compare the performance of adaptive meshes, we compute errors of numerical solutions by different meshes. The adaptive meshes are generated from Mesh D with 8, 16 or 32 partitions per unit length as initial meshes. Errors by different meshes are presented in Figure 3, where we observe all meshes result in the consistent rates with the error estimate in Section 4; the rate for the velocity is optimal, $O(h^2)$, in the L^2 -norm, and the rates for viscous and polymeric stresses, and pressure are suboptimal, O(h), in the L^2 -norm. However, the ALS method using Mesh A improves convergence rates over other two meshes as shown in Figure 3.

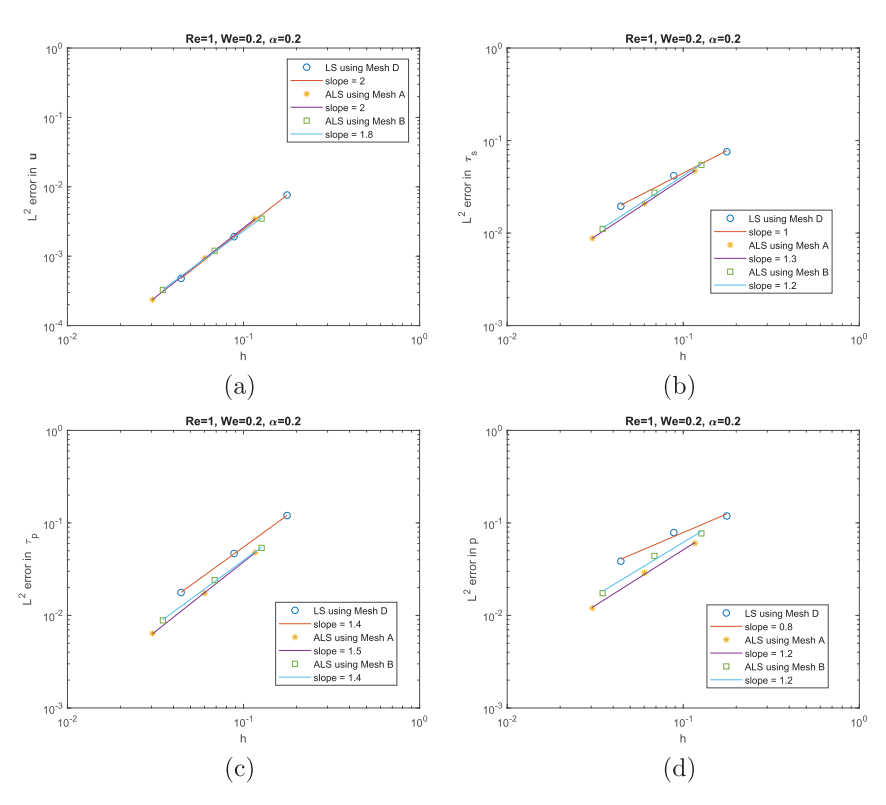


Figure 3. L^2 errors of (a) **u**, (b) τ_s , (c) τ_p , and (d) p by different meshes, Mesh D (°), Mesh A (*), and Mesh B (\square).

5.2. Problem 2

Consider the Giesekus model in a 4-to-1 contraction domain of an upstream channel that abruptly narrows to a channel one quarter of the original width with x (the flow direction) for $-5 \le x \le 5$, and the contraction occurring at x = 0. The width of upstream channel is 1; thus the downstream width is 1/4. Let $\mathbf{u} = (u_1, u_2)$ and $\boldsymbol{\tau}_p$ be specified on the inflow boundaries, $\mathbf{u} = \mathbf{0}$ on the wall boundaries, and $u_2 = 0$ on the outflow boundary. Pressure p is set to zero at the point where the outflow boundary meets the symmetry boundary, and u_2 and $\boldsymbol{\tau}_{p_{xy}}$ vanish on the symmetry boundary, which are the same conditions used in [5,9]. The forcing function \mathbf{f} in (5) is set to $\mathbf{0}$. The model equations (5)–(8) are simulated with the fixed value for β , $\beta = 1/9$, and various other parameter values in the range of $0.1 < Re < 10, 0.1 < \alpha < 1$, and 0.1 < We < 1.5, respectively.

The meshes considered are listed in Table 1 and illustrated in Figure 4. Uniform criss-crossed Mesh X in Figure 4(a) is a mesh generated by using Delaunay triangular grids with 16 partitions per unit length. Mesh H in Figure 4(b) is an initial mesh generated by aligning the longest edges of these triangular grids of Mesh X along the same direction of downstream for $x \in [0.065, 5]$. Mesh U in Figure 4(c) is a uniformly refined mesh of Mesh H. The adaptive mesh shown in Figure 4(d) is a local refinement of Mesh H, and the longest edges of its triangular grids are aligned in the diagonal direction downstream of $x \in [0.065, 5]$.

5.2.1. Parameter selection for weights on uniform meshes

To study the performance of Newton LS iteration scheme (28), we start with a uniform mesh for the model with (*Re*, *We*, α) = (1, 0.2, 0.2), and s = 0 for the weight W = (1 + We + $s\alpha$)² in (19).

Mesh DOF Type Uniform criss-crossed mesh 6400 3377 Н 6400 3377 Uniform mesh U Uniform refined mesh 25,600 116,556 Adaptive mesh by |u| 9989 45,983 Adaptive mesh by $g^{1/2}$

12,932

59,550

Table 1. Meshes considered for (*Re, We,* α) = (1, 0.2, 0.2).

^bDegrees of freedom (DOF) is at the final refinement step (S).

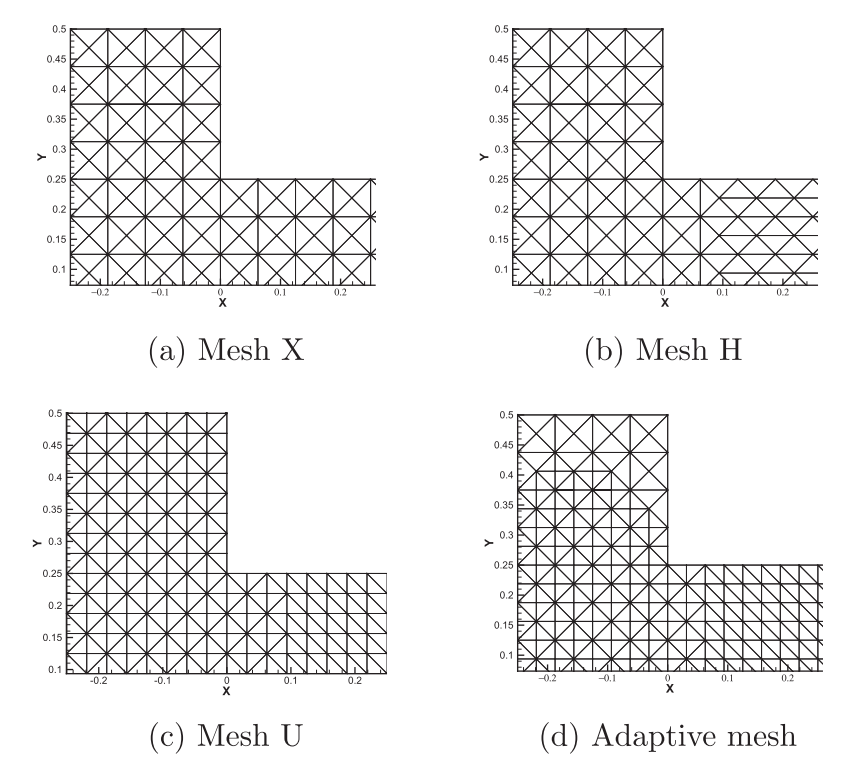


Figure 4. Description of mesh refinements. (a) Input Mesh X with 16 partitions per unit length is a uniform criss-crossed mesh. (b) Uniform Mesh H is an initial mesh generated by Mesh X. (c) Mesh U is a uniformly refined mesh of Mesh H. (d) Adaptive mesh is a locally refined mesh of Mesh H.

First, the weight $K = 10^m$ in (17) is chosen by the same way considered for Problem 1 using Mesh H as the initial mesh. We investigate the convergence of the functional $g^{1/2}$ in (30) by varying m. Figure 5 shows $\delta g_m^{1/2}$ for different m values ranging from 4 to 10 for the fixed parameters (Re, We, α) = (1, We, 0.2) and various We, We = 0.2, 0.5, 1 and 1.5. Using the same criterion described for Problem 1, we observe that convergence is achieved at m = 9, therefore, the mass conservation weight $K = 10^9$ is used in the LS formulation for all computations for Problem 2. Figure 5 also shows that the number of iteration steps increases with increasing We. This indicates that for high We flows, the convergence of the iteration is lost and the Jacobian matrix becomes singular, as demonstrated in [8].

^aN represents the number of elements.

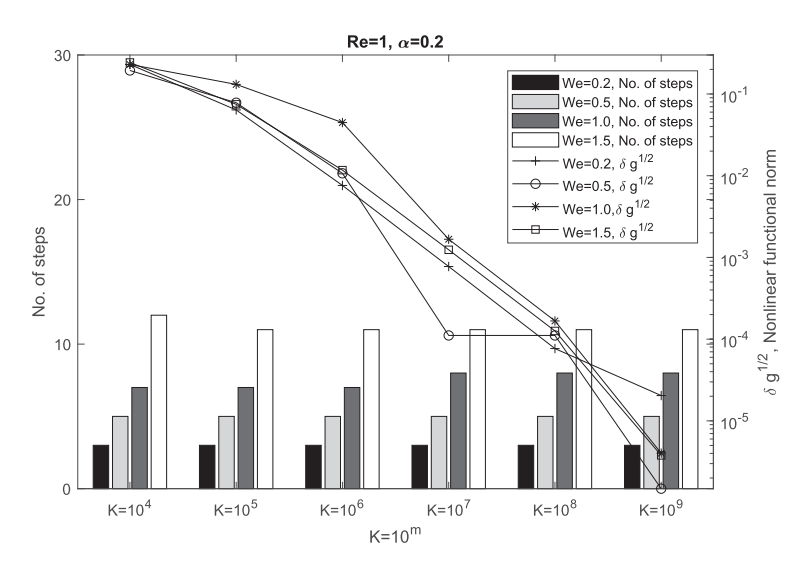


Figure 5. Nonlinear functional norm $\delta g_m^{1/2}$ in nested iteration for various weights $K=10^m$ ($4 \le m \le 10$) at (Re, We, α) = (1, We, 0.2) with We=0.2, 0.5, 1 and 1.5. Here No. of steps represents the number of Newton iterations for convergence.

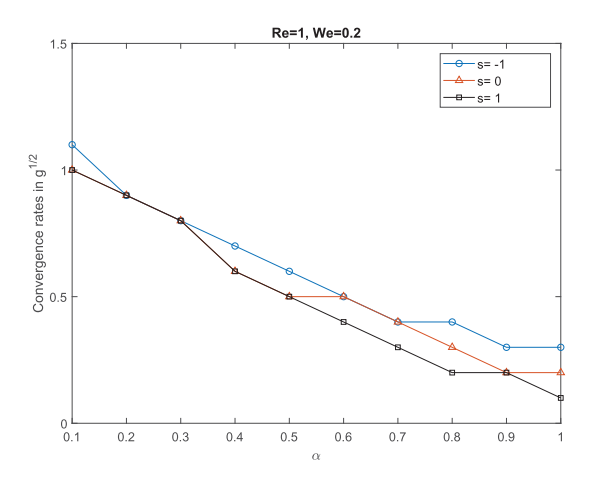


Figure 6. Convergence rates of the LS solutions with $W=(1+We+s\alpha)^2$ for s=-1, 0, 1 when (*Re, We,* α) = (1, 0.2, α) for $0.1 \le \alpha \le 1$.

Next, we study a selection of s for the weight $W = (1 + We + s\alpha)^2$, where the parameter is in the range of $-1 \le s \le 1$. In [10], the weight W with s = 1 is chosen to solve the PTT viscoelastic fluid flows past a transverse slot. Now, in order to select the optimal parameter, we investigate convergence rates of the LS solutions with s = -1, 0 and 1 on uniformly refined meshes. Figure 6 presents convergence rates of $g^{1/2}$ at (*Re*, *We*, α) = (1, 0.2, α), where α ranges from 0.1 to 1. The figure shows that the functional $g^{1/2}$ of the LS solution achieves the expected rate, O(h), at the lowest α , 0.1, and convergence rates decrease with an increase in α . The weight W with s=-1 improves the rate of convergence compared with W with s = 0 and 1. Therefore, we use the coefficient s = -1 in the weight W for the LS functional (17) in all following experiments.

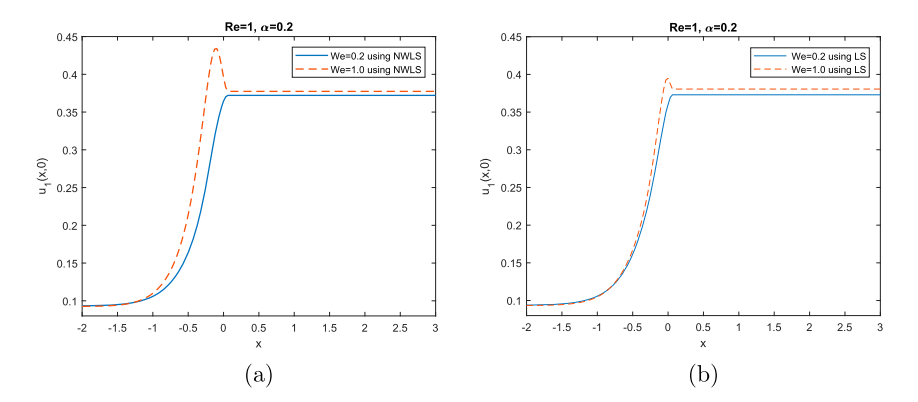


Figure 7. Comparison of horizontal velocities $u_1(x, 0)$ along y = 0 on Mesh U: (a) NWLS and (b) LS.

Next, using the fixed weights W, K chosen above, we compare horizontal velocities by the LS method and NWLS [5] on uniform Mesh U, respectively. Figure 7(a) and (b) present the horizontal velocity u_1 profiles along the axis of symmetry (y = 0) for We = 0.2 and 1. For the value of We = 1, we observe that the peak in the NWLS solution Figure 7(a) is higher than that of the LS solution (Figure 7 b). We notice that the peak height of velocity increases for higher values of We, which could attribute to the existence of corner singularity in a high We fluid. Though there seems to exist an elasticity effect in the prediction of velocity profile, for a high We fluid, the velocity near the reentrant corner of the NWLS is more sensitive than that of the LS method. Our results show that using the LS method, the peak height generated near the corner can be reduced from 0.434 (NWLS) to 0.395 (LS) as shown in Figure 7(b). Therefore, the LS method reduces the influence of corner singularities in a high We fluid better than the NWLS method.

5.2.2. Computational grids

We now consider the LS method in (28) using the adaptive mesh approach described in Section 4 and name it the ALS method. Meshes A and B illustrated in Figure 8(a) and (b) are generated using magnitudes of velocity $|\mathbf{u}|$ and the nonlinear LS functional norm $g^{1/2}$, respectively, with (Re, We, α) = (1, 0.2, 0.2). Using the same stopping criterion in Section 5.1, we obtain mesh convergence after two mesh refinement steps. These adaptive meshes are highly refined near the downstream boundary layers, exhibiting a refined region close to the corner. In contrast to the results in [3,12], systematic mesh refinements near the reentrant corner are necessary for avoiding a substantial increase in the number of unknown factors. Thus Meshes A and B match the expected mesh refinements in the corner region. In addition, as shown in Table 1, using Mesh A, the number of elements can be reduced from 12932 (Mesh B) to 9989 (Mesh A). Thus adaptive Mesh A is more efficient than other meshes. Further, we present contours of $|\mathbf{u}|$ and $g^{1/2}$ on Meshes A and B in Figure 8. Figure 8(c) and (d) show similar contours of $|\mathbf{u}|$, and as shown in Figure 8(e) and (f), the a-posteriori error $g^{1/2}$ near the corner can be decreased by using Mesh A. Thus the adaptive Mesh A can reduce the influence of corner singularities.

We also investigate convergence rates of $g^{1/2}$ by the LS method using Mesh U and by the ALS method using Meshes A and B for various We values. Figure 9 presents convergence rates of $g^{1/2}$ at $(Re, We, \alpha) = (1, We, 0.2)$ with We = 0.2, 0.5, 1 and 1.5. The figure shows that the rates approach to O(h) for Meshes A and B, but only $O(h^{1/2})$ for Mesh U, and the expected optimal convergence rates in $g^{1/2}$ of O(h) can be restored with adaptive meshes. The ALS using Mesh A improves the rate of convergence compared with the ALS using Mesh B and the LS using Mesh U. Moreover, the average convergence rate of $g^{1/2}$ for the ALS using Mesh A is close to 1.5, which is much higher than the



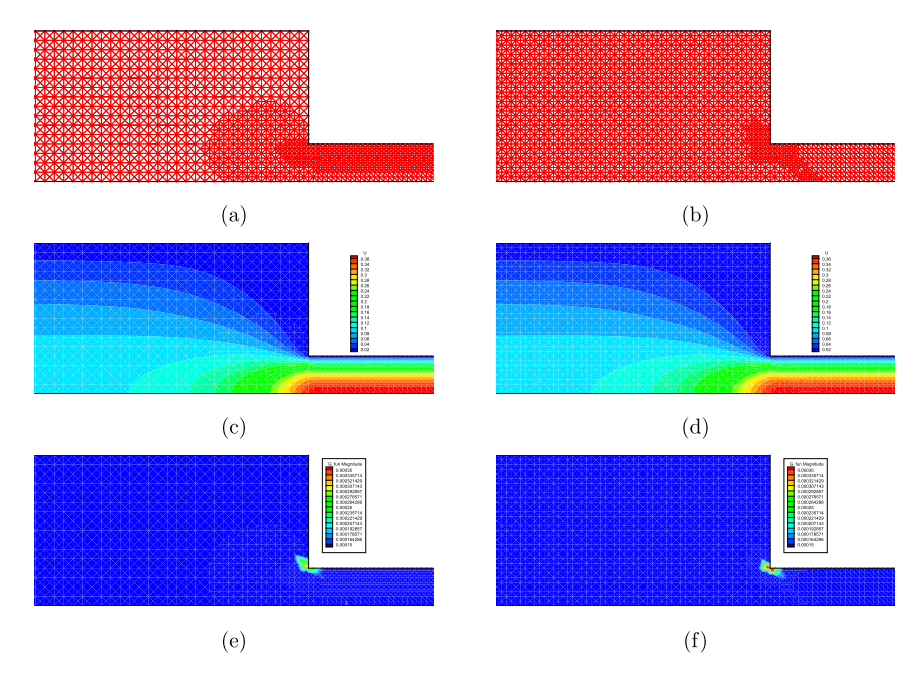


Figure 8. Convergent adaptive meshes in two iterations, plots of velocity magnitude and $g^{1/2}$ for (*Re*, We, α) = (1, 0.2, 0.2). (a) Mesh A, (b) Mesh B, (c) Magnitude of velocity on Mesh A, (d) Magnitude of velocity on Mesh B, (e) Plot of $g^{1/2}$ on Mesh B.

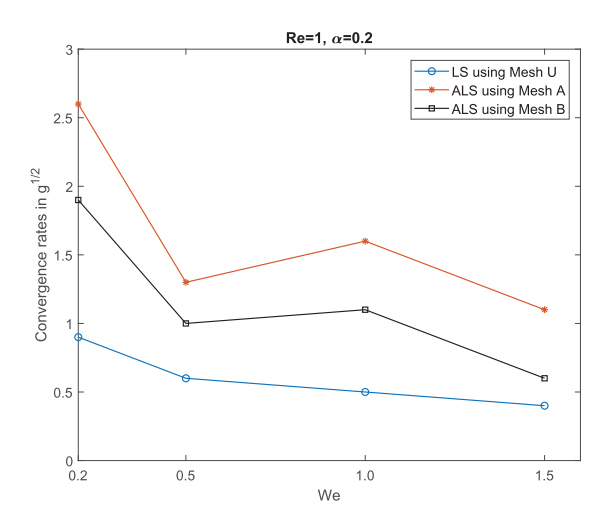


Figure 9. Convergence rates of the LS solutions in $g^{1/2}$ at (*Re*, *We*, α) = (1, *We*, 0.2) with We = 0.2, 0.5, 1 and 1.5.

expected rate O(h). Figure 10 shows the horizontal velocity $u_1(5, y)$ profiles at We = 0.2 and 1 by the ALS method on Meshes A and B, and by the LS method on Mesh U, respectively. The results seem to be in agreement for both values of We. However, as shown in Table 1, using the ALS scheme, the number of elements can be reduced from 25,600 (Mesh U) to 9989 (Mesh A) or to 12,932 (Mesh

14 HSUEH-CHEN LEE AND H. LEE

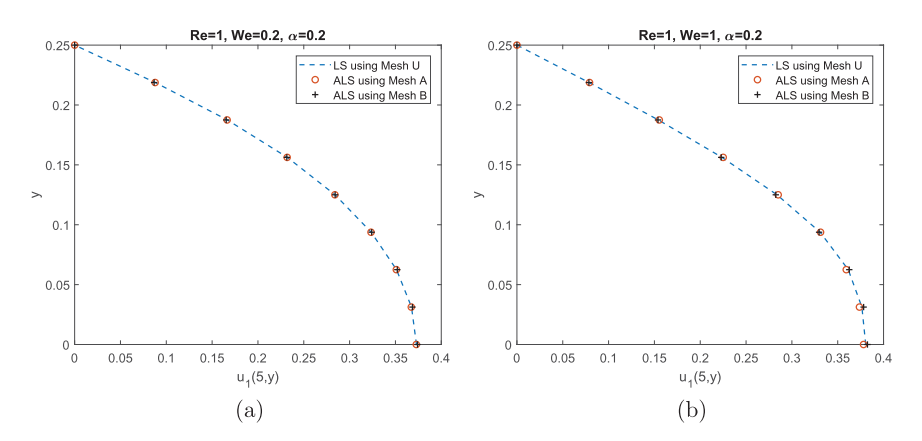


Figure 10. Horizontal velocity $u_1(5, y)$ along the outlet at (a) (Re, We, α) = (1, 0.2, 0.2) and (b) (Re, Re, RR, RR,

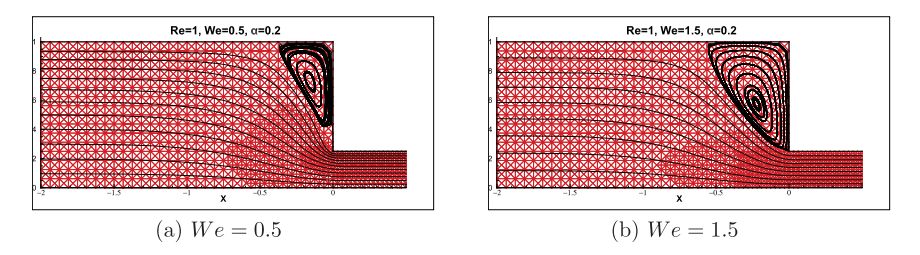


Figure 11. Adaptive Mesh A and streamlines for (a) We = 0.5 and (b) We = 1.5 at $(Re, We, \alpha) = (1, We, 0.2)$.

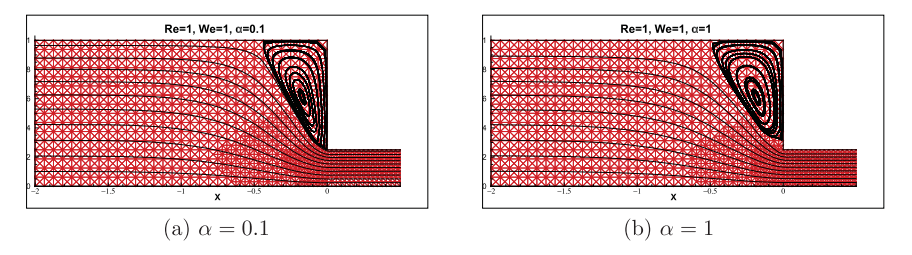


Figure 12. Adaptive Mesh A and streamlines for (a) $\alpha = 0.1$ and (b) $\alpha = 1$ at (*Re*, *We*, α) = (1, 1, α).

B). Thus the ALS method on Mesh A is more efficient than the LS method on Mush U or the ALS method on Mesh B. Hence, we use the velocity magnitude gradient $|\mathbf{u}|$ as the grading refined function to generate Mesh A for the ALS method in the next experiments.

5.2.3. Effects of physical parameters

We investigate the effects of model parameters, We, α and Re on Mesh A by varying each parameter while the other two are fixed. Streamlines of the flow at $(Re, We, \alpha) = (1, We, 0.2)$ and $(Re, We, \alpha) = (1, 1, \alpha)$ are presented in Figures 11 and 12, respectively, for We = 0.5, 1.5, and $\alpha = 0.1, 1$. To study the effect of inertia, we use Re = 0.1 and 10 in the model with (We, α) set to (1, 0.2). Streamlines are shown in Figure 13 for this case. Figures show that the adaptive meshes are dependent on the physical behaviours and refined along the large variation area of the flow. In



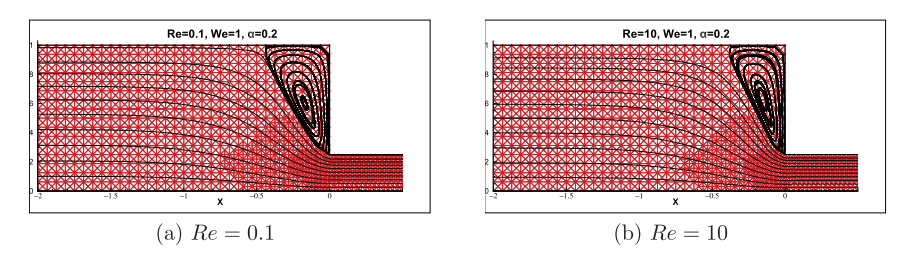


Figure 13. Adaptive Mesh A and streamlines for (a) Re = 0.1 and (b) Re = 10 at $(Re, We, \alpha) = (Re, 1, 0.2)$.

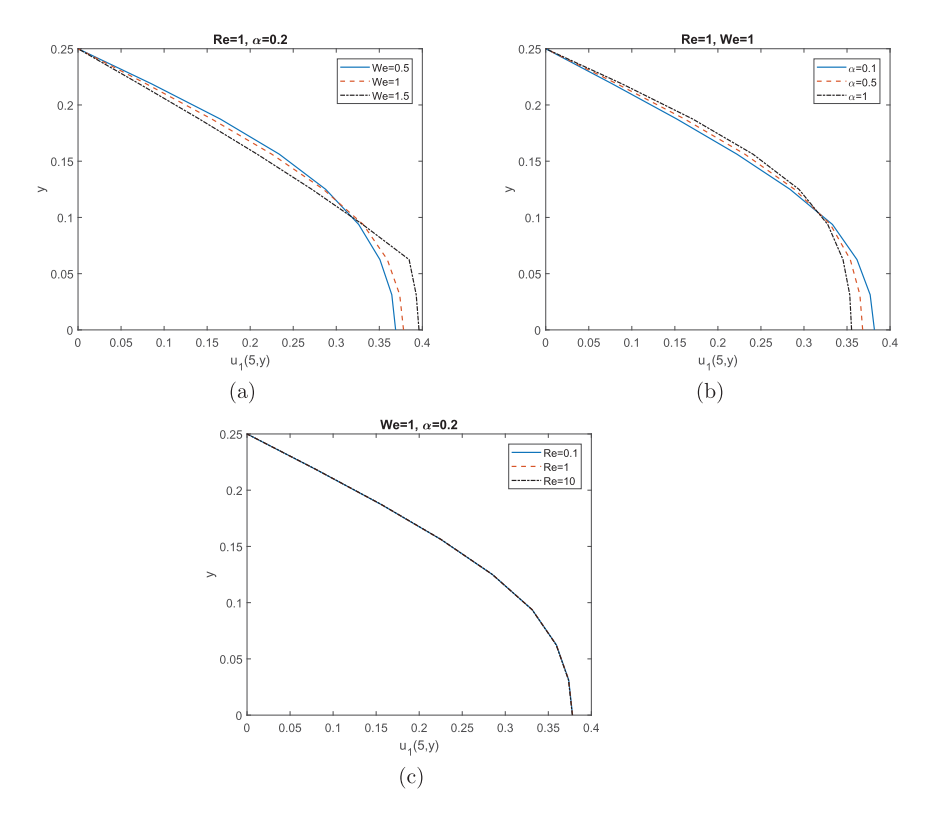


Figure 14. Horizontal velocity $u_1(5, y)$ on Mesh A at (a) (*Re, We,* α) = (1, *We,* 0.2) for We = 0.5, 1, 1.5, (b) (*Re, We,* α) = (1, 1, α) for $\alpha = 0.1, 0.5, 1$ and (c) (*Re*, *We*, α) = (*Re*, 1, 0.2) for *Re* = 0.1, 1, 10.

addition, we observe the presence of a larger recirculation region near the top corner for the higher We, α and lower Re values.

Figure 14 presents the effects of physical parameters on the horizontal velocity component, u_1 at the outlet (x = 5). Figure 14(a) displays $u_1(5, y)$ for We = 0.5, 1 and 1.5 when $(Re, \alpha) = (1, 0.2)$. We observe that when We = 0.5, the horizontal velocity of the fluid near the wall is higher than those of other values of We, resulting in a similar parabolic velocity profile at the outlet. Because the low We fluid near the wall has a low polymeric viscosity as shown in [9], the growth rate of the velocity away from the wall is higher than that of the high We fluid. When We increases, its effects become more dominant, and the profiles at the outlet exhibit shapes of sharper parabola (We = 0.5).

Moreover, the profiles by the ALS method are similar to those by the NWLS [9] for the Oldroyd-B model. To evaluate the effect of mobility factor α , we consider $\alpha=0.1$, 0.5 and 1 with (Re, We)=(1, 1) for plots in Figure 14(b). The results indicate that when $\alpha=1$, the fluid velocity near the wall is higher than those of other values of α , thus a flat velocity profile at the outlet is observed. Because the mobility factor α controls the shear-thinning behaviour of the fluid [7], the high α fluid near the wall has a low viscosity; the growth rate of the velocity away from the wall of the high α fluid is greater than that of the low α fluid. The effect of α on the velocity field is very similar to that of the Carreau time constant illustrated by the NWLS [14] for the shear-thinning Carreau fluid. For Re=0.1, 1 and 10 with fixed $(We, \alpha)=(1, 0.2)$ we obtain almost identical profiles of u_1 at the outlet as shown in Figure 14(c).

6. Conclusion

We proposed an adaptive LS (ALS) method for the Giesekus model, where a grading function of the LS solution is used for adaptive mesh refinement. We considered two stabilized weights for the ALS method to prevent loss of mass conservation and improve convergence of a solution at high We and α . The weight on mass conservation term is adjusted based on a residual-type a-posteriori error estimator $g^{1/2}$ for the LS functional, while a weighting function involving We and α is used for the constitutive equation. Coefficients of the weighting function are adjusted to reflect the physical behaviour of the fluid and improve the convergence rate of the ALS method. We provided an error estimate for the linearized viscoelastic system and presented numerical results supporting the estimate. We demonstrated that the results of the ALS method are consistent with those of the NWLS method presented in [5], and in the presence of corner singularity, the effect of high Weissenberg number can be reduced by using the ALS method. For the ALS approach the magnitudes of velocity and a nonlinear LS functional norm $g^{1/2}$ were used to calculate the grading function to adaptively refine a mesh and capture the flow region. Using continuous piecewise linear finite element spaces for all variables and appropriately weighting the continuity and constitutive equations, we obtained the first-order convergence rate for $g^{1/2}$ by the ALS method, which is higher than the rates by the LS method on uniform meshes. In the study of model parameters by the proposed method, it was observed that the effect of We is more dominant for a high We, and the shear-thinning behaviour of the fluid increases with an increasing α . In addition, the effects of inertia can be neglected in viscoelastic fluid flows at low Re.

The method developed in this study is an original combination of novel and existing techniques that aims to address shortcomings of the LS method for the 4-to-1 planar contraction flow problem. The proposed method resolves the difficulties related to the presence of corner singularities in this specific numerical example and computational limitations arising from the exorbitant number of unknowns. Moreover, when compared to the LS method on a uniform mesh, the ALS approach with adaptive mesh refinements improves the convergence rate as well as computational efficiency by the use of less elements. Future studies can extend our approach to more physically realistic domains, including more complex geometries and unsteady flows, and compare our results with experimental findings. A combination of grading functions will be implemented to model flows in various physical settings. These capabilities will be added to the proposed method to address more complex tests. These issues will be investigated further in future implementations.

Acknowledgments

The first author gratefully acknowledges the financial support provided in part by the Ministry of Science and Technology of Taiwan under grant 109-2115-M-160-001. The second author is grateful for the financial support provided in part by the US National Science Foundation under grant DMS-1818842.



Disclosure statement

No potential conflict of interest was reported by the author(s).

References

- [1] M.A. Alves, P.J. Oliveira, and F.T. Pinho, Benchmark solutions for the flow of Oldroyd-B and PTT fluids in planar contractions, J. Non-Newton. Fluid Mech. 110 (2003), pp. 45-75.
- [2] R.B. Bird, R.C. Armstrong, and O. Hassager, Fluid Mechanics, Dynamics of Polymeric Liquids, Volume 1: Fluid Mechanics, 2nd ed., John Wiley and Sons, New York, 1987.
- [3] Z. Cai and C.R. Westphal, An adaptive mixed least-squares finite element method for viscoelastic fluids of Oldroyd type, J. Non-Newton. Fluid Mech. 159 (2009), pp. 72-80.
- [4] O.M. Coronado, D. Arora, M. Behr, and M. Pasquali, Four-field Galerkin/least-squares formulation for viscoelastic fluids, J. Non-Newton. Fluid Mech. 140 (2006), pp. 132-144.
- [5] T.F. Chen, C.L. Cox, H.C. Lee, and K.L. Tung, Least-squares finite element methods for generalized Newtonian and viscoelastic flows, Appl. Numer. Math. 60 (2010), pp. 1024-1040.
- [6] J.H. Chaudhry, S.D. Bond, and L.N. Olson, A weighted adaptive least-squares finite element method for the Poisson-Boltzmann equation, Appl. Math. Comput. 218 (2012), pp. 4892-4902.
- [7] H. Giesekus, A simple constitutive equation for polymer fluids based on the concept of deformation-dependent tonsorial mobility, J. Non-Newton. Fluid Mech. 11 (1982), pp. 69-109.
- [8] R. Keunings, On the high Weissenberg number problem, J. Non-Newton. Fluid Mech. 20 (1986), pp. 209-226.
- [9] H.C. Lee, A nonlinear weighted least-squares finite element method for the Oldroyd-B viscoelastic flow, Appl. Math. Comput. 219 (2012), pp. 421-434.
- [10] H.C. Lee and H. Lee, Numerical simulations of viscoelastic fluid flows past a transverse slot using least-squares finite element methods, J. Sci. Comput. 79 (2019), pp. 369-388.
- [11] J.L. Liu, Exact a posteriori error analysis of the least squares finite element method, Appl. Math. Comput. 116 (2000), pp. 297-305.
- [12] H.C. Lee, An adaptively refined least-squares finite element method for generalized Newtonian fluid flows using the Carreau model, SIAM J. Sci. Comput. 36 (2014), pp. 193-218.
- [13] H.C. Lee and T.F. Chen, Adaptive least-squares finite element approximations to Stokes equations, J. Comput. Appl. Math. 280 (2015), pp. 396-424.
- [14] H.C. Lee, A nonlinear weighted least-squares finite element method for the Carreau-Yasuda non-Newtonian model, J. Math. Anal. Appl. 432 (2015), pp. 844-861.
- [15] H.C. Lee, Adaptive weights for mass conservation in a least-squares finite element method, Int. J. Comput. Math. 95 (2018), pp. 20-35.
- [16] M.T. Ravanchi, M. Mirzazadeh, and F. Rashidi, Flow of Giesekus viscoelastic fluid in a concentric annulus with inner cylinder rotation, Int. J. Heat Fluid Flow 28 (2007), pp. 838-845.
- [17] N. Thongjub, B. Puangkird, and V. Ngamaramvaranggul, Slip effect study of 4:1 contraction flow for Oldroyd-B model, Int. J. Math., Comput. Phys., Elect. Comput. Eng. 7 (2013), pp. 1334-1341.
- [18] S. Zhou and L. Hou, A weighted least-squares finite element method for Phan-Thien-Tanner viscoelastic fluid, J. Math. Anal. Appl. 436 (2016), pp. 66-78.